Int. J. Electrochem. Sci., 8 **(2013)** 446 - 457

International Journal of
ELECTROCHEMICAL
SCIENCE
www.electrochemsci.org

Effects of Pyran-Ring Structure in Carbon Sources on the Electrochemical Performance of $LiFePO_4$/C

Baohua Li[1,*], *Yutao Xing*[1,2], *Xiaodong Chu*[1], *Jun Ma*[1], *Yan-Bing He*[1],*Dengyun zhai*[1], *Hongda Du*[1], *Chunguang Wei*[1,2], *Hongzhou Chen*[1,2] *and Feiyu Kang*[1,2]

[1] Key Laboratory of Thermal Management Engineering and Materials, Graduate School at Shenzhen, Tsinghua University, Shenzhen, Guangdong Province, 518055, P. R. China
[2] Department of Materials Science & Engineering, Tsinghua University, Beijing, 100084, P. R. China.
[*]E-mail: libh@sz.tsinghua.edu.cn

Received: 23 September 2012 / *Accepted:* 28 November 2012 / *Published:* 1 January 2013

Nano-sized $LiFePO_4$/C (LFP/C) with excellent electrochemical performance was prepared by using carbon precursors with different pyran-ring structures as carbon sources. The effects of pyran-ring structure on the electrochemical performance of LFP/C composites were extensively investigated. Results show that LFP/C using starch with many pyran rings exhibits a specific capacity of 105 $mAhg^{-1}$ at current density of 2550 mAg^{-1} (15 C). This capacity is much higher than those of using glucose with one pyran ring and lauric acid without pyran-ring structure, whose capacities are 86 $mAhg^{-1}$ and 80 $mAhg^{-1}$ at current density of 2550 mAg^{-1}, respectively. The great improvement is mainly attributed to the pyran-ring structure of the carbon sources. The degree of graphitization of the pyrolysed carbon increases with increase in the number of pyran rings in the carbon sources, which dramatically improves the electrical conductivity of the LFP/C to reduce the charge-transfer resistance. Thus, the LFP/C using starch as carbon source presents the best electrochemical performance.

Keywords: Pyran ring; Carbon sources; $LiFePO_4$/C; Cathode material; Lithium ion batteries

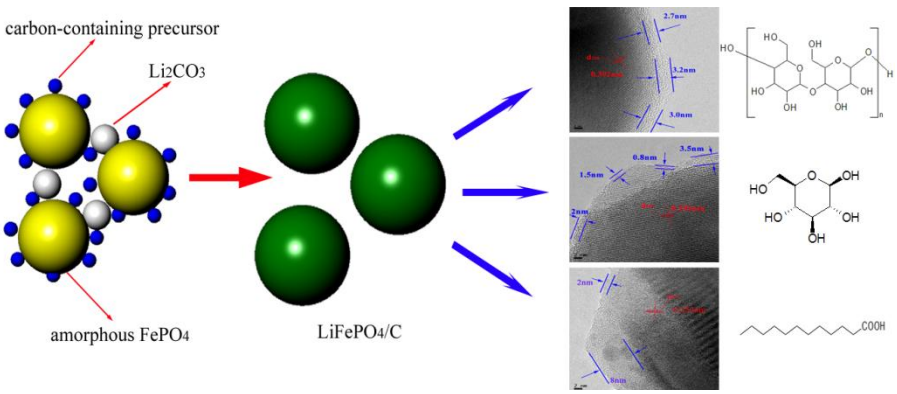

1. INTRODUCTION

Olivine $LiFePO_4$ (LFP) is considered as one of the most promising cathode materials for lithium ion batteries (LIBs) [1]. Compared with the conventional $LiCoO_2$, LFP has many advantages [2-4], such as environmental friendliness, thermal stability, non-toxicity, low cost, and high safety. However, the intrinsic disadvantages such as low electrical conductivity and slow lithium-ion diffusion dramatically have hindered its large-scale applications [1, 4, 5]. Considerable effects have been done to overcome and alleviate them, of which carbon coating on surface of LFP particles is one of the most common and effective methods to achieve the high rate charge/discharge performance of LFP [6-10]. Carbon coating can greatly increase the electrical conductivity, effectively reduce the particle size [11] and thus dramatically improve the electrochemical performance [12]. Furthermore, carbon coating is favorable on preventing the oxidation of Fe^{2+} to some degree [13]. The previous researches [14-17] indicate that carbon sources with different molecule structures have different coating effects and degree of graphitization of the pyrolysed carbon, which results in different electrical conductivities and electrochemical performances of LFP/C cathode materials. Therefore, the selection of suitable carbon source with unique molecular structure is critical to preparing LFP/C with excellent performance. Previous studies showed that a polymeric carbon has a higher ratio of graphitized carbon than by other organic precursors [17-19], which is beneficial to improve the electrical conductivity. In addition, it was found that polymers with functionalized aromatic are more favorable for graphitization than polymers without [20-22]. This demonstrates that the structure and functional group of organic precursors may play an important role in the improvement of electrical conductivity and electrochemical performance of $LiFePO_4$/C.

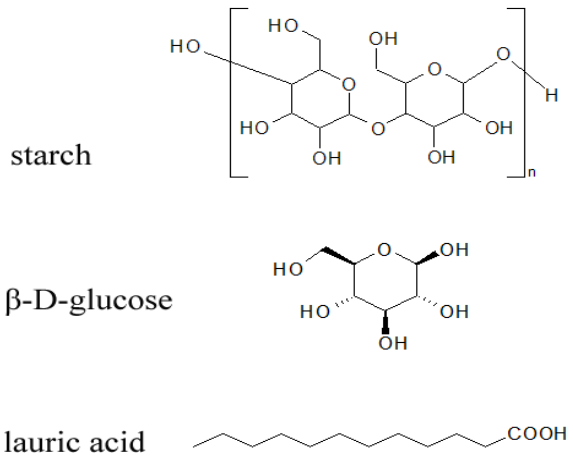

Figure 1. Structures of starch, β-D-glucose and lauric acid.

Recently, carbon precursors with pyran-ring structure (such as glucose, starch) were used widely to synthesize the LFP/C that exhibited good electrochemical performance[23-25]; however, to date, there are few studies referring to the effects of pyran rings in carbon sources on the performance of LFP/C. Herein we selected water-soluble starch (many pyran rings in the molecule), β-D-glucose

(one pyran ring in the molecule) and lauric acid (without pyran-ring in the molecule) as shown in Fig. 1 as the carbon sources to investigate the effects of the pyran rings on the structure and performance of LFP/C via a precipitation-carbothermal method. It is found that the pyran-ring structure has a significant effect on the thickness and graphitization degree of coated carbon, and hence results in a quite different electrochemical performance of LFP/C.

2. EXPERIMENTAL

2.1 Synthesis of amorphous $FePO_4$

The amorphous $FePO_4$ was synthesized using $FeCl_3 \cdot 6H_2O$ and $(NH_4)_2HPO_4$ (both from Analytical Regent, AR) as the reactants with a molar ratio of 1:1. Cetyltrimethyl Ammonium Bromide (CTAB) used as a surfactant aqueous solution (0.05mol/L) was added to the reactor to restrain the agglomeration of the particles. Then， an aqueous NH_4OH solution (25 wt.%) was also dropped to adjust the pH value of the solution to ~ 2. Lastly, the as-obtained amorphous iron phosphate was filtered, washed, and dried under 353 K (80 ^oC) for 12 h and homogeneous powders were obtained.

2.2 Preparation of LFP/C

The as-prepared $FePO_4$ powders were mixed with Li_2CO_3 (AR), carbon sources (starch, glucose, lauric acid) (AR) by ball milling for 5 h in ethanol solution. The precursors were pre-sintered at 350 ^oC for 10 h and then heated at 650 ^oC for 15 h in Ar atmosphere to obtain LFP/C. Three LFP/C samples using starch, glucose, and lauric acid as the carbon sources were denoted as LFP-S, LFP-G, and LFP-L, respectively.

2.3 Material characterization and electrochemical evaluation

The phase composition of products was characterized by powder X-ray diffraction (XRD) using a Rigaku diffractometer (D/MAX-2500, Japan) equipped with Cu-Kα radiation. Field emission scanning electron microscopy (FESEM, HITACH S4800, Japan) was used to observe the morphology of the samples. The high-resolution images of the samples were obtained by a high resolution transmission electron microscope (HRTEM, JEOL-2011, Japan). A simultaneous thermogravimetric analysis and differential scanning calorimeter (TG-DSC) apparatus (Netzsch STA 449C, Germany) were used for thermal analysis of the samples at a heating rate of 10 ^oC/min under Ar atmosphere. TG analysis was also used for the determination of carbon content in LFP/C under air environment. The carbon state in LFP/C samples was characterized using a Raman spectrometer (Renishaw Invia Reflex, Britain) with a 514 nm Ar-ion laser. The electrical conductivity was measured by the ST-2258A multifunction digital four-probe tester, in which the sample was pressed into a thin plate.

CR2032 coin cells were assembled to test the electrochemical properties of the LFP/C. The as-prepared LFP/C was used as cathode and Li metal as anode. The 1M $LiPF_6$ solution in a mixture

solvent of ethylene carbonate, ethylene methyl carbonate and dimethyl carbonate (EC/EMC/DEC 1:1:1 by volume) was used as electrolyte and polypropylene (Celgard 2500, Celgard Inc., USA) as separator. The cathode is composed of 80 wt.% LFP/C composite powders, 10 wt.% acetylene black and 10 wt.% polyvinylidene fluoride (PVDF). The mixture containing LFP/C, acetylene black and PVDF was blended in N-Methyl Pyrrolidone (NMP) to obtain the mixed slurry, which was coated on stainless aluminum substrate, and dried in vacuum for 8 h at 85 °C. The cells were assembled in an argon-filled glove box. The cells were cycled between 2.3 V and 4.5 V (vs. Li/Li^+) at a constant current mode with various charge and discharge rates using a LAND CT2001 apparatus (China). The EIS measurement was carried out by IM6ex electrochemical work station from 0.1 HZ to 500 KHZ at amplitude of 5 mV.

3. RESULTS AND DISCUSSION

3.1 Material preparation and characterization

Fig. 2a shows the XRD patterns of the as-obtained $FePO_4$ precursor and its crystallized product after sintered at 500 ^oC. It is found that the XRD pattern of the sintered $FePO_4$ product is in accordance with the pattern of JPDS card No. 84-0876, which confirms that the sintered product is hexagonal $FePO_4$. Accordingly, it can be further proved that the obtained $FePO_4$ precursor is amorphous. The XRD patterns of LFP/C composite (prepared by using the prepared amorphous $FePO_4$, Li_2CO_3 and carbon precursors) as given in Fig. 2b are in accordance with the typical orthorhombic LFP pattern of JPDS card No. 83-2092, which indicates that the LFP with good crystalline was successfully synthesized. There are no peaks corresponding to carbon found in the diffraction pattern. This is probably due to the low content and uncrystalline state of carbon.

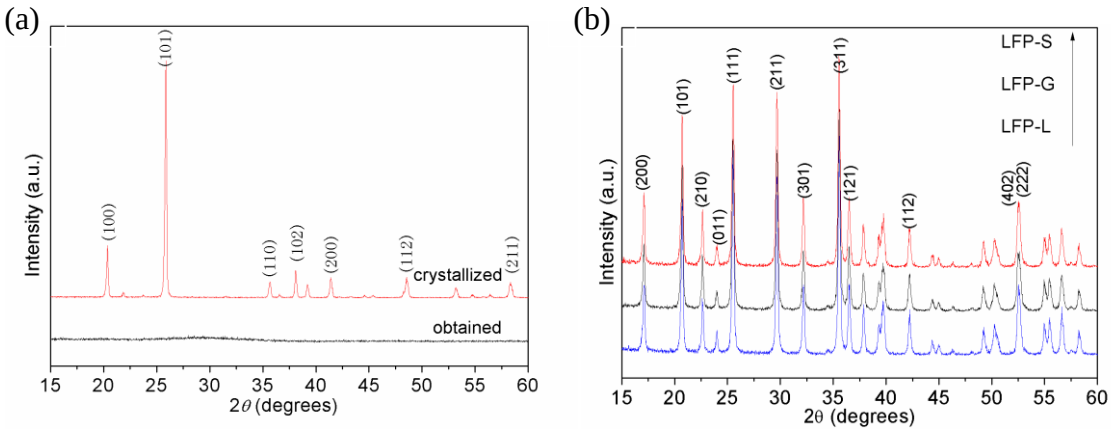

Figure 2. XRD patterns of (a) as-obtained and crystallized $FePO_4$ and (b) LFP/C composites of LFP-S, LFP-G and LFP-L.

The SEM image of the prepared amorphous $FePO_4$ at room temperature as shown in the inset of Fig. 3a indicates that the amorphous $FePO_4$ consists of uniform spherical nano-particles with size

less than 50 nm. The size distribution of amorphous $FePO_4$ particles as showed in Fig. 4a is uniform in the range of 18~34 nm. The SEM images of LFP-S, LFP-G, and LFP-L are showed in Figs. 3a, 3c and 3e, respectively. It is found that LFP-S has the minimum average particle size and the least particle agglomerations. Particle size distributions of the three samples are displayed in Figs. 4b-4d. The LFP-S has a mean particle size of 80.5 nm in the range of 50-120 nm, while LFP-G has a mean particle size of 100.8 nm in the range of 70-150 nm and LFP-L has a mean particle size of 102.8 nm in the range of 50-160 nm.

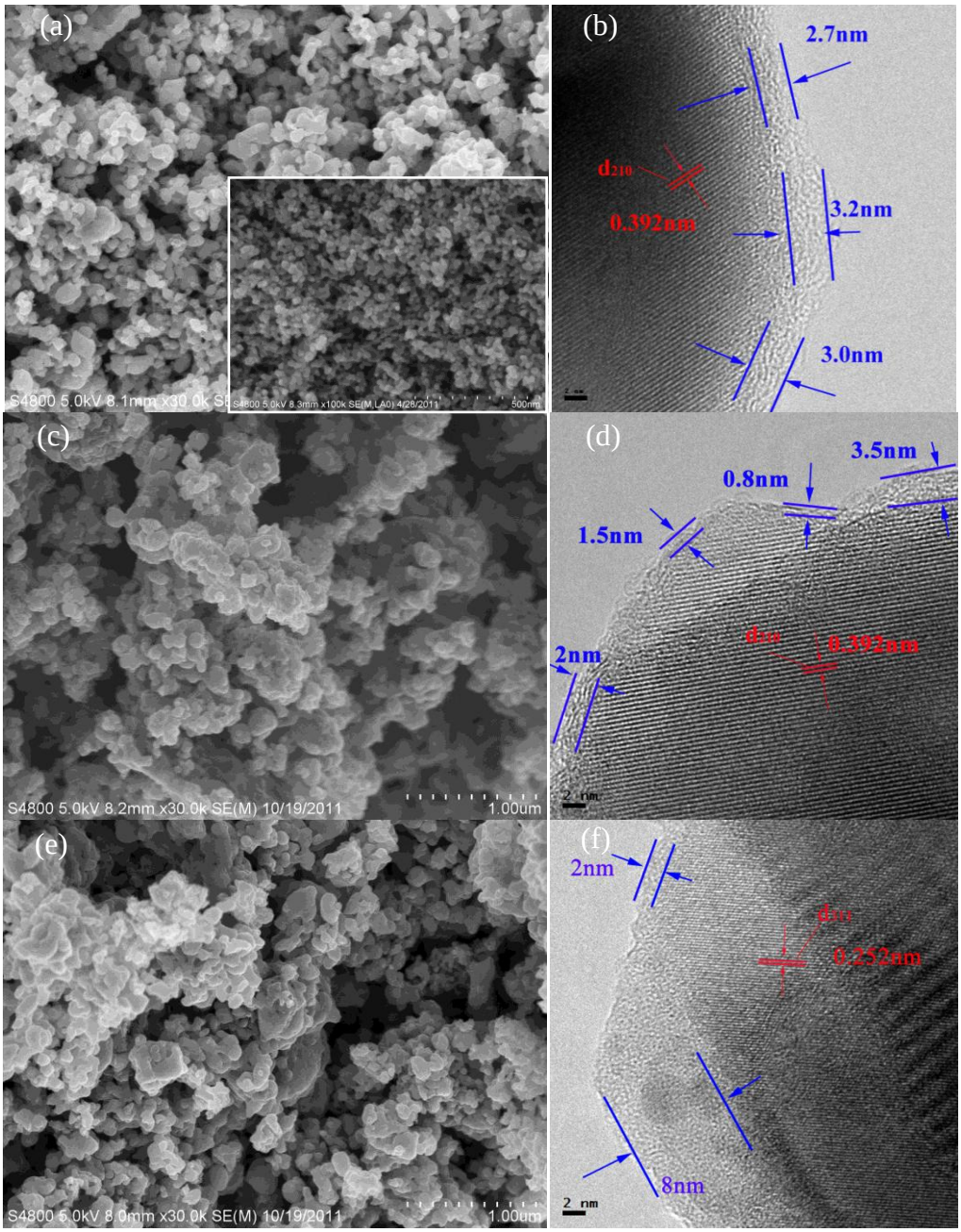

Figure 3. Left: SEM images of (a) LFP-S, (c) LFP-G, and (e) LFP-L. Right: HRTEM images of (b) LFP-S, (d) LFP-G, and (f) LFP-L. The SEM image of amorphous $FePO_4$ is shown as inset in (a).

Apparently, LFP-S has a comparatively smaller size and a narrower band in size distribution than those of LFP-G and LFP-L. The smaller particle size and narrower band in size distribution are favorable to reducing the transport distance for electrons and Li-ions to attain the high-rate capacities of LFP/C composite. Thus, it is suggested that starch with many pyran rings can inhibit the agglomeration of particles more effectively than other carbon sources with only one (glucose) or no (lauric acid) pyran rings in the structure of molecules.

The high resolution TEM images of the LFP-S, LFP-G and LFP-L samples shown Figs. 4b, 4d and 4f, respectively, clearly indicate that all LFP samples have well crystalline structure with a carbon layer on the particle surface, whereas, the carbon layer on the LFP surface exhibits quite different thickness and uniformity. It is seen that the LFP-S has a more uniform carbon coating layer of 2-3 nm in thickness than those of LFP-G and LFP-L, which may be the main reason for the smaller particle size of LFP-S. An incomplete carbon coating layer may lead to particle growing. A fully uniform carbon coating on LFP surface will highly enhance the electrical conductivity (shown in table 1). This is attributed to the formation of good conducting network that promotes the transfer of electrons along all directions during charge and discharge [26]. On the contrary, non-uniform (too thick) carbon coatings will result in obstruction for Li^+ insertion and extraction which would cause slower lithium ion diffusion [27]. The pyran rings in the polymer favor the formation of uniform thickness carbon coatings on the LFP to enhance the conductivity and diffusion of lithium ions.

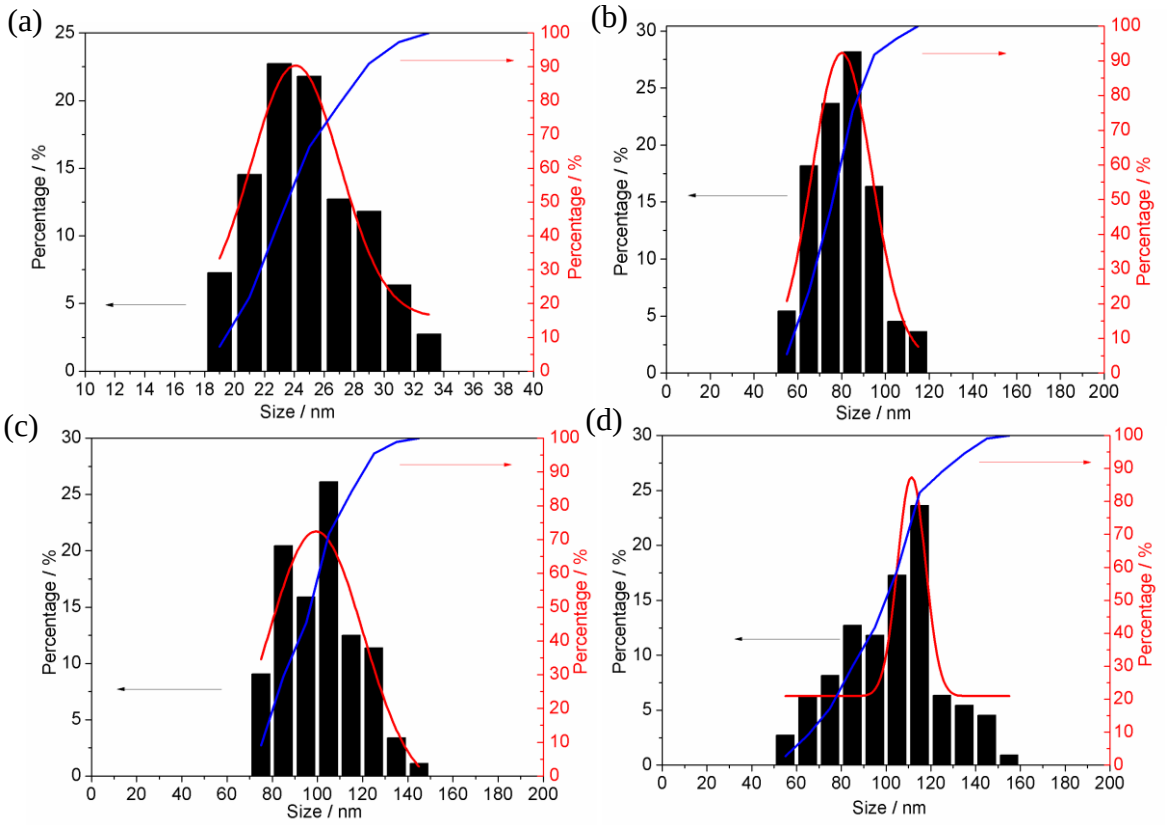

Figure 4. Particle size distributions of (a) amorphous $FePO_4$, (b) LFP-S, (c) LFP-G, and (d) LFP-L

Fig. 5a exhibits the TG and DSC curves of the mixture of $FePO_4$, Li_2CO_3 and glucose. (The TG and DSC curves using two other carbon sources are similar to glucose, not shown here.) The endothermic DSC peak at 125 ^oC is attributed to the loss of crystal water in $FePO_4$ precursor, Li_2CO_3 and glucose. The weight loss in TG curve below 200 ^oC is mainly resulted from the release of the physically absorbed water and crystal water. The exothermic peak around 260 ^oC may be resulted from the decomposition of glucose, which corresponds to the weight loss in TG curves from 220 ^oC to 300 ^oC. The obviously exothermic DSC peak at 450 ^oC signatures the formation of LFP. Therefore, the precursors of $FePO_4$, Li_2CO_3 and glucose are pre-sintered at 350 ^oC for the decomposition of the organic precursor and calcinated at temperature of 650 ^oC for the complete crystallization of LFP.

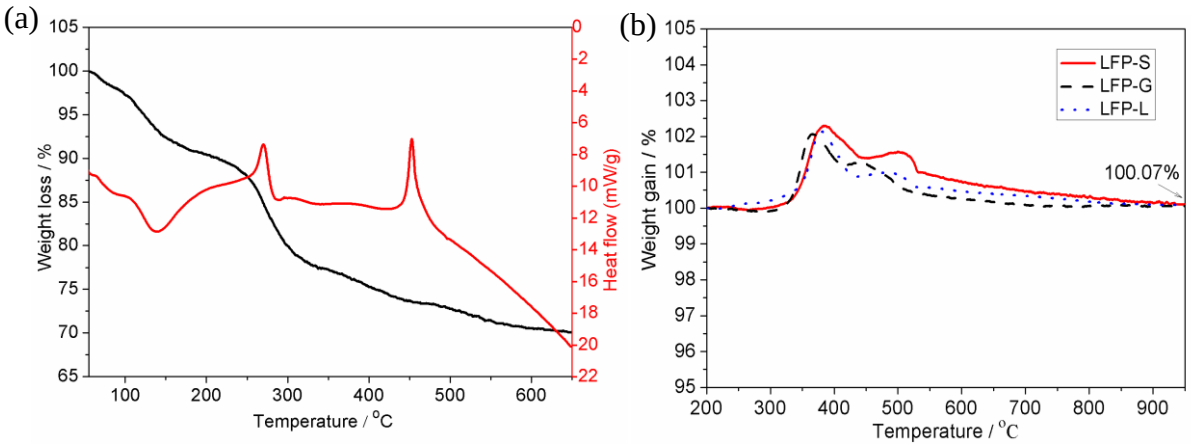

Figure 5. (a) TG and DSC curves of the mixture of $FePO_4$, Li_2CO_3 and glucose in Ar atmosphere at the heating rate of 10℃/min and (b) TG curves of LFP/C in air atmosphere at a heating rate of 10℃/min.

The content of residual carbon in the LFP-S, LFP-G and LFP-L samples is determined by performing TG in air atmosphere. LFP is oxidized above 450 ^oC in air which brings a weight gain of 5.07 wt.%, and the remaining carbon is transformed to CO_2 above 550 ^oC [28]. Both Fig. 5b and Table 1 indicate that the carbon content of the three samples was all about 5.0 wt. %.

Table 1. Physical and electrochemical properties for the three samples of $LiFePO_4$/C

sample	Carbon content (wt. %)	I_D/I_G	conductivity (S/cm)
LFP-S	4.97	1.46	7.69×10^{-4}
LFP-G	5.02	1.56	3.27×10^{-4}
LFP-L	4.98	2.49	1.30×10^{-4}

3.2 Effects of carbon sources on the performance of LFP

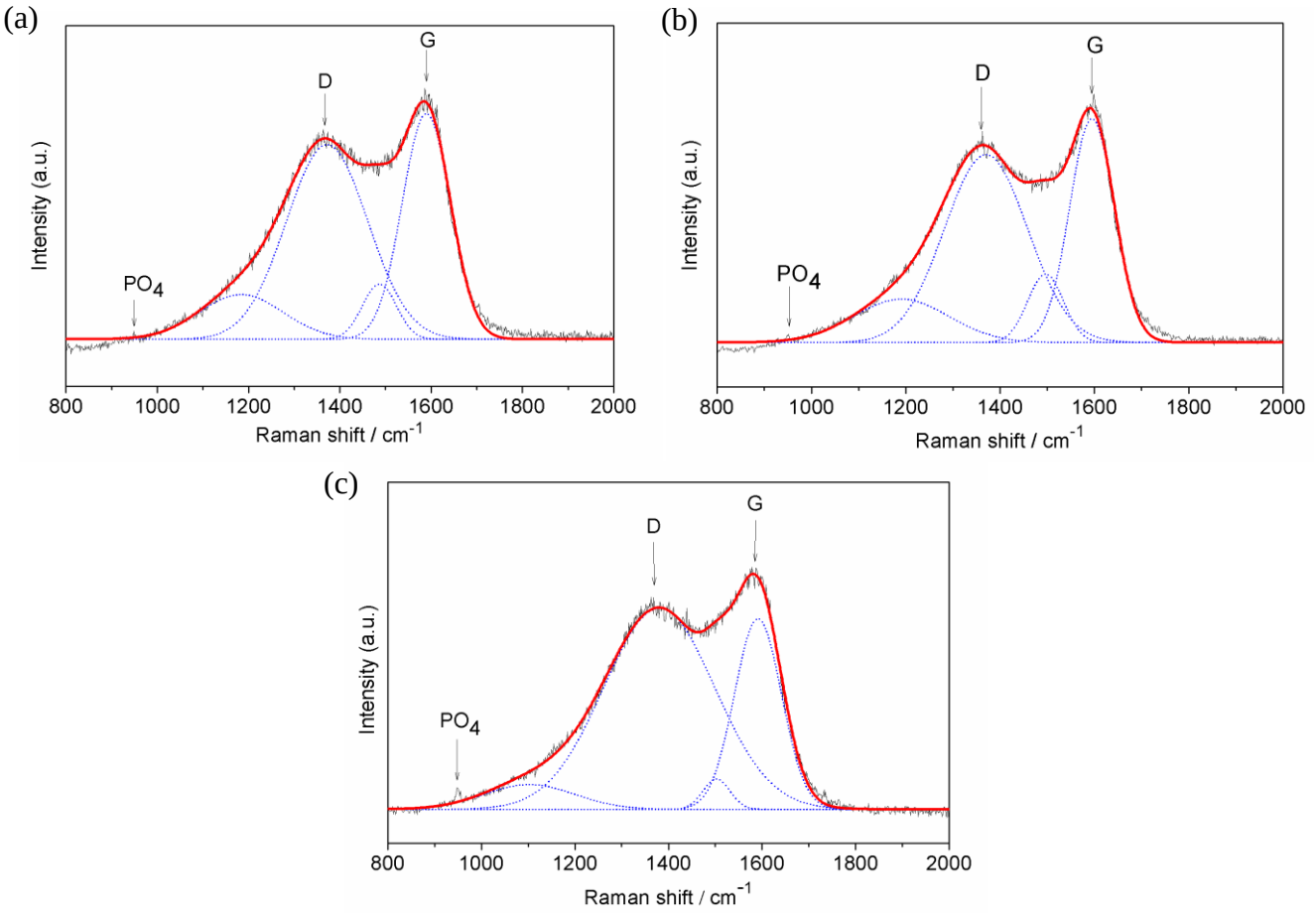

Figure 6. Raman spectra of (a) LFP-S, (b) LFP-G, and (c) LFP-L.

The Raman spectroscopy is used to characterize the structure of pyrolysed carbon in LFP/C. Fig. 6 shows the Raman spectra of LFP-S, LFP-G and LFP-L. All spectra consist of a relatively small band at 940 cm^{-1} corresponding to symmetric PO_4 stretching model of LFP [20]. Two intense broad peaks at about 1350 cm^{-1} and 1585 cm^{-1} are ascribed, respectively, to the D and G bands of pyrolysed carbon in the LFP/C composite [29]. The D and G bands are composed of four signals located at 1194, 1347, 1510, 1585 cm^{-1} [22, 29, 30]. The bands at 1347 and 1585 cm^{-1} have been assigned to the sp^2 graphite-like structure, whereas all other bands are attributed to the sp^3 type carbon, which are often observed in amorphous carbonaceous materials. The band positions (Fig. 6) were slightly different from previous values. Therefore, it is difficult to establish an accurate quantitative relationship among the three samples, whereas a semi-quantitative discussion is viable. The estimated ratio of sp^2/sp^3 is about 4~10 for all the samples, indicating that the fraction of graphite-like carbon was above 80% and the conducting path was constructed by the graphite-like carbon. The ratio I_D/I_G of the carbon coating used to analyze the degree of graphitization, which has a great influence on the electrical conductivity and electrochemical performance of LFP [31, 32]. The ratio I_D/I_G of the three samples was listed in Table 1. It can be found that the LFP-S has the lowest I_D/I_G value among the samples, indicating the highest degree of graphitization of the pyrolysed carbon using starch with many pyran rings as

compared to other carbon sources. The high degree of graphitization in pyrolysed carbon can improve the conductivity of LFP/C composite to result in higher electrochemical performance.. The structural difference among three pyrolysed carbon precursors depends highly on the graphitization process at high temperature. The carbon precursors with aromatic functional structure would facilitate the graphitization of carbon to enhance the electrochemical performance of electrode materials [20, 21]. During the decomposition process, the pyran rings of starch would breakdown to become large conjugated aromatic structures above 600 ^{o}C [33]. This forms high graphitized carbon in pyrolysed carbon.

Raman spectroscopy is a light scattering technique and is sensitive to the surface topology of the sample. The intensity of carbon to PO_4 bands [$I_{(D+G)}/I_{PO4}$] can be used as a criteria to determine the coating effect of pyrolysed carbon over the LFP/C composite. The value of $I_{(D+G)}/I_{PO4}$ is mainly related to two factors that are the total amount of pyrolysed carbon in the composite and the distribution of carbon on the surface of LFP. Therefore, a higher intensity of $I_{(D+G)}/I_{PO4}$ in LFP-S (shown in Fig. 6) means a more uniform coating of carbon with high conducting path over LFP/C particles, corresponding to the carbon distribution in the TEM images shown in Fig. 3. This suggests that the pyran-ring structure would favor the graphitized carbon after sintering at high temperature above 600 ^{o}C.

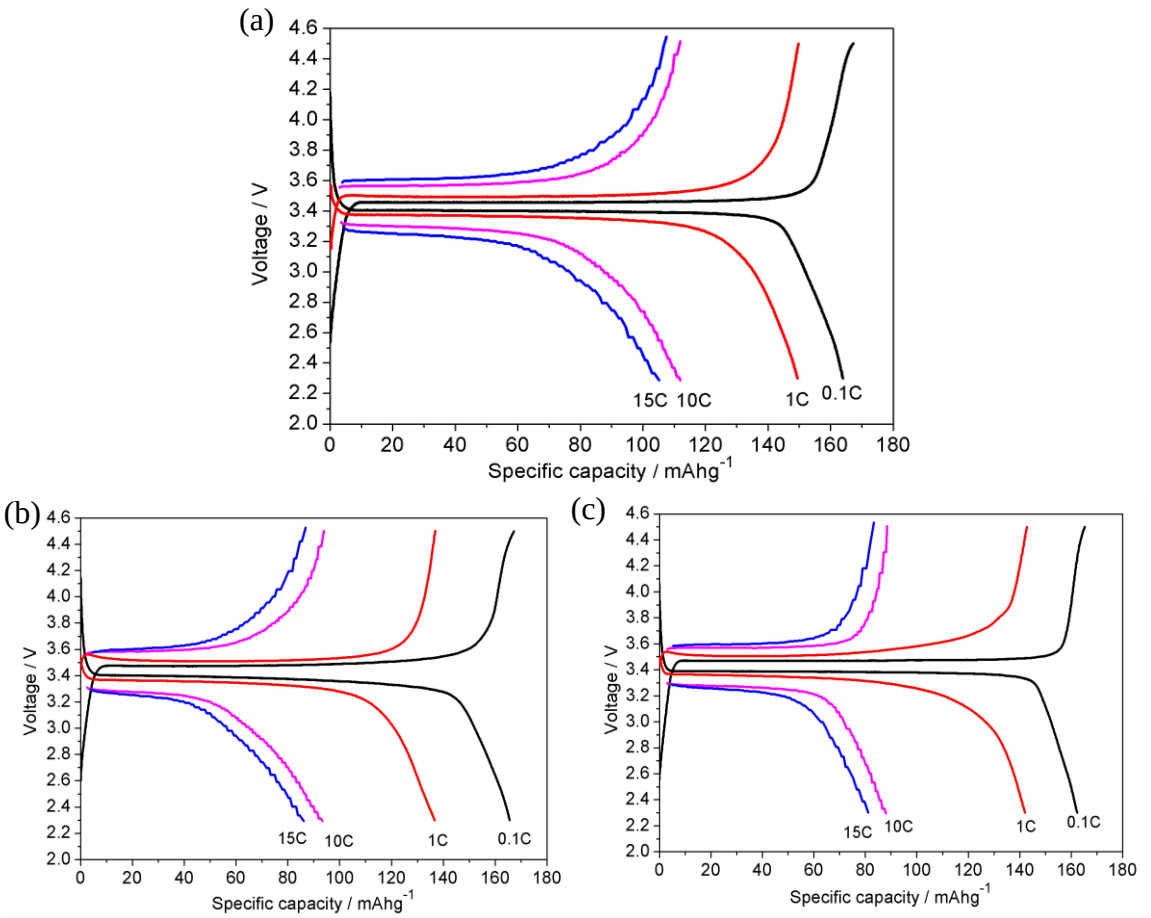

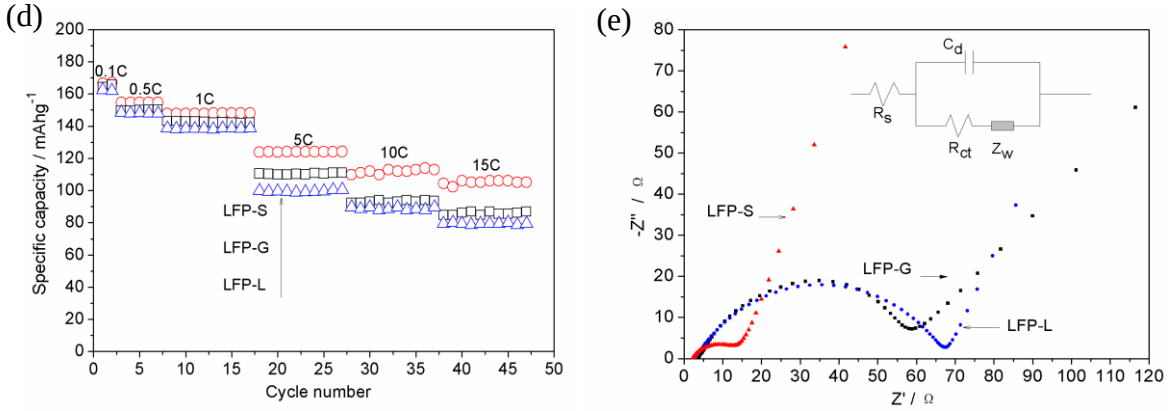

Figure 7. Charge and discharge curves of (a) LFP-S (b) LFP-G (c) LFP-L at different rate; (d) discharge capacity at different rates of three LFP/C samples; (e) electrochemical impedance spectra (EIS) for LFP/C after 10 cycles of charge and discharge at 0.1 C.

Figs. 7a-7c present the galvanostatic charge and discharge curves of the prepared LFP-S, LFP-G and LFP-L at different charge-discharge current density at 25 ^{o}C. From Fig. 7d, the measured specific capacities of LFP-S, LFP-G and LFP-L at rate of 0.1 C are 166, 165 and 163 mAhg^{-1}, respectively, which are close to the theoretical capacity of 170 mAhg^{-1}. In addition, the LFP-S has a charge/discharge profile gap narrower ($\Delta E < 0.1V$) than those of LFP-G and LFP-L (see Figs. 7a-7c), demonstrating a lower electrochemical reaction resistance of the LFP-S electrode. The gap of charge/discharge voltage profile becomes wider due to polarization with the increases in the charge/discharge current density. LFP-S exhibits the best high rate performance, which can deliver 114 and 105 mAhg^{-1} at the current density of 1700 mAg^{-1} (10 C) and 2550 mAg^{-1} (15 C), respectively (Fig. 7d). For LFP-G and LFP-L, their capacities are 86 mAhg^{-1} and 80 mAhg^{-1} at 2550 mAg^{-1} (15 C), respectively. This is coherent with the particle size of LFP/C composite, carbon distribution and structure of carbon coatings on the surface of the three samples.

Fig. 7e displays the Nyquist plots of electrochemical impedance spectrum (EIS) of coin cells using the three samples as the cathode materials. The plot consists of a depressed semicircle at the high frequency and a straight line at the low frequency. An equivalent circuit is also showed in Fig. 7e, where R_s, C_d, R_{ct} and Z_w represent ohmic resistance, capacitance of double layer, charge-transfer resistance, and Warburg impedance, respectively [34, 35]. The values of R_{ct} that equals approximately to the diameter of the semicircle in the high frequency region are 16 Ω, 60 Ω and 68 Ω for the three samples of LFP-S, LFP-G and LFP-L, respectively. The LFP-S electrode, which has the lowest charge transfer resistance in the electrochemical reactions during the charge/discharge process, may contribute to the high rate charge/discharge performance.

4. CONCLUSIONS

In this work, nano-sized LFP/C with excellent high-rate electrochemical performances was successfully synthesized using carbon precursor with different structures. LFP/C using starch with

many pyran rings as carbon sources exhibits the highest discharge capacity, as compared to those using glucose with one pyran ring in the molecule and lauric acid without pyran-ring structure. The carbon source with structure of more pyran-rings results in smaller particle size, uniform coating thickness, lower I_D/I_G ratio, higher electrical conductivity and lower charge-transfer resistance, and hence leads to the better electrochemical performance. The pyran-ring structure benefits the formation of large conjugated aromatic structure at high temperature that accounts for the high graphitized degree of pyrolysed carbon in LFP/C.

ACKNOWLEDGEMENTS
This work was supported by National Nature Science Foundation of China (No.51072131 and 51232005), Shenzhen Technical Plan Project, Key Project for Basic Research for three main areas of Shenzhen (No.JC201005270288A and JC201104210152A), Guangdong Province Innovation R&D Team Plan for Energy and Environmental Materials (No.2009010025) and China Postdoctoral Science Foundation (No. 2012M510022).

References

1. A.K. Padhi, K.S. Nanjundaswamy, J.B. Goodenough, *J. Electrochem. Soc*., 144 (1997) 1188-1194.
2. Y. Wang, J. Wang, J. Yang, Y. Nuli, *Advanced Functional Materials*, 16 (2006) 2135-2140.
3. B.L. Ellis, W.R.M. Makahnouk, Y. Makimura, K. Toghill, L.F. Nazar, *Nature Materials*, 6 (2007) 749-753.
4. Y. Wang, Y. Wang, E. Hosono, K. Wang, H. Zhou, *Angewandte Chemie-International Edition*, 47 (2008) 7461-7465.
5. C. Delmas, M. Maccario, L. Croguennec, F. Le Cras, F. Weill, *Nature Materials*, 7 (2008) 665-671.
6. K.A. Seid, J.C. Badot, O. Dubrunfaut, S. Levasseur, D. Guyomard, B. Lestriez, *Journal of Materials Chemistry*, 22 (2012) 2641-2649.
7. D. Lepage, C. Michot, G. Liang, M. Gauthier, S.B. Schougaard, *Angewandte Chemie-International Edition*, 50 (2011) 6884-6887.
8. X. Lou, Y. Zhang, *Journal of Materials Chemistry*, 21 (2011) 4156-4160.
9. S.W. Oh, S.-T. Myung, S.-M. Oh, K.H. Oh, K. Amine, B. Scrosati, Y.-K. Sun, *Advanced Materials*, 22 (2010) 4842-+.
10. Y. Wu, Z. Wen, J. Li, *Advanced Materials*, 23 (2011) 1126-1129.
11. S.A. Needham, A. Calka, G.X. Wang, A. Mosbah, H.K. Liu, *Electrochemistry Communications*, 8 (2006) 434-438.
12. W.-J. Zhang, *Journal of Power Sources*, 196 (2010) 2962-2970.
13. K. Wang, R. Cai, T. Yuan, X. Yu, R. Ran, Z. Shao, *Electrochimica Acta*, 54 (2009) 2861-2868.
14. Z.-Y. Chen, H.-L. Zhu, S. Ji, R. Fakir, V. Linkov, *Solid State Ionics*, 179 (2008) 1810-1815.
15. C. Lai, Q. Xu, H. Ge, G. Zhou, J. Xie, *Solid State Ioni*cs, 179 (2008) 1736-1739.
16. Z.Y. Tang, Y.L. Ruan, *Acta Chimica Sinica*, 63 (2005) 1500-1504.
17. Y.M. Bai, H. Chen, S.C. Han, Russ. *J. Electrochem*., 47 (2011) 84-88.
18. M.S. Pan, J.C. Liu, Z.T. Zhou, C. Peec-Org, Structure and Electrochemical Properties of LiFePO(4)/C with Different Disordered/Graphitized Carbon, Sci Res Publ, Inc-Srp, Irvin, 2010.
19. S. Yu, S. Dan, G. Luo, W. Liu, Y. Luo, X. Yu, Y. Fang, *J. Solid State Electrochem*., 16 (2012) 1675-1681.
20. Y.-H. Nien, J.R. Carey, J.-S. Chen, *Journal of Power Sources*, 193 (2009) 822-827.

21. C.-W. Ong, Y.-K. Lin, J.-S. Chen, *Journal of The Electrochemical Society*, 154 (2007) A527-A533.
22. Y.Q. Hu, M.M. Doeff, R. Kostecki, R. Finones, *Journal of The Electrochemical Society*, 151 (2004) A1279-A1285.
23. L.-B. Kong, P. Zhang, M.-C. Liu, H. Liu, Y.-C. Luo, L. Kang, *Electrochimica Acta*, 70 (2012) 19-24.
24. M. Pan, Z. Zhou, *Materials Letters*, 65 (2011) 1131-1133.
25. S. Wang, C. Zhou, Q. Zhou, G. Ni, J. Wu, *Journal of Power Sources*, 196 (2011) 5143-5146.
26. J. Wang, X. Sun, *Energy & Environmental Science*, 5 (2012) 5163-5185.
27. Y.-D. Cho, G.T.-K. Fey, H.-M. Kao, *Journal of Power Sources*, 189 (2009) 256-262.
28. I. Belharouak, C. Johnson, K. Amine, *Electrochem. Commun*., 7 (2005) 983-988.
29. M.M. Doeff, Y.Q. Hu, F. McLarnon, R. Kostecki, ELECTROCHEMICAL AND SOLID STATE LETTERS, 6 (2003) A207-A209.
30. O. Chi-Wi, L. Yuan-Kai, C. Jenn-Shing, *Journal of The Electrochemical Society*, 154 (2007).
31. Y. Lin, M.X. Gao, D. Zhu, Y.F. Liu, H.G. Pan, *Journal of Power Sources*, 184 (2008) 444-448.
32. J.-H. Lin, J.-S. Chen, *Electrochimica Acta*, 62 (2012) 461-467.
33. X.Q. Zhang, J. Golding, I. Burgar, *Polymer*, 43 (2002) 5791-5796.
34. K. Yang, Z. Lin, X. Hu, Z. Deng, J. Suo, *Electrochimica Acta*, 56 (2010) 2941-2946.
35. X. Li, F. Kang, X. Bai, W. Shen, *Electrochem. Commun*., 9 (2007) 663-666